

## MERIDIONAL CIRCULATION VARIABILITY FROM LARGE-APERTURE RING-DIAGRAM ANALYSIS OF GLOBAL OSCILLATION NETWORK GROUP AND MICHELSON DOPPLER IMAGER DATA

I. GONZÁLEZ HERNÁNDEZ, R. KOMM, F. HILL, AND R. HOWE  
National Solar Observatory,<sup>1</sup> 950 North Cherry Avenue, Tucson, AZ 85719; irenegh@nso.edu

T. CORBARD  
Observatoire de la Côte d’Azur, Nice, France

AND

D. A. HABER  
JILA, University of Colorado, Boulder, CO 80309  
Received 2005 September 6; accepted 2005 October 6

### ABSTRACT

Ring-diagram analysis, a local helioseismology technique, has proven to be very useful for studying solar sub-surface velocity flows down to a depth of about  $0.97 R_{\odot}$ . The depth range is determined by the modes used in this type of analysis, and thus depends on the size of the area analyzed. Extending the area allows us to detect lower spherical harmonic degree ( $l$ ) modes which, at a constant frequency, penetrate deeper in the Sun. However, there is a compromise between the size of the area and the validity of the plane-wave approximation used by the technique. We present the results of applying the ring diagrams to  $30^{\circ}$  diameter areas over the solar surface in an attempt to reach deeper into the solar interior. Meridional flows for 25 consecutive Carrington rotations (1985–2009) are derived by applying this technique to Global Oscillation Network Group (GONG) and Michelson Doppler Imager (MDI) data. This covers a time span of almost 2 yr, starting at the beginning of 2002. The amplitude of the meridional flow shows a variation of the order of  $5 \text{ m s}^{-1}$  during this period. Our results indicate that the flows increase toward the interior of the Sun for the depth range studied. We find a 1 yr periodicity in the appearance of an equatorward meridional cell at high latitudes that coincides with maximum values of the solar inclination toward the Earth ( $B_0$  angle).

*Subject headings:* Sun: helioseismology — Sun: interior — Sun: oscillations

### 1. INTRODUCTION

Recent dynamo models include, along with the  $\Omega$  and the  $\alpha$  effects, a meridional circulation component, in order to reproduce the solar cycle (Dikpati & Gilman 2001). Several theoretical models have been proposed for the meridional motions. Gilman & Miesch (2004) proposed that the meridional circulation cannot penetrate below  $0.7 R_{\odot}$ , while previous works by Nandy & Choudhuri (2002) suggested a deeper circulation, which penetrates into the stable layers below the convection zone.

From the observational point of view, different methods have produced a variety of results. Magnetic feature tracking (Komm et al. 1993; Snodgrass & Dailey 1996), Doppler measurements (Hathaway et al. 1996; Nesme-Ribes et al. 1997), and helioseismology (Giles et al. 1997; Haber et al. 2002) agree on a maximum surface amplitude of about  $10\text{--}20 \text{ m s}^{-1}$ . However, the latitudinal position of the maximum amplitude, the temporal variability, and the depth profile of these flows varies substantially between techniques. The time-distance technique has indicated a subsurface, reverse meridional flow cell developing at higher latitudes during the rising phase of the solar magnetic cycle (Giles 2000). Haber et al. (2002) also found an equatorward meridional cell above  $30^{\circ}$  in the northern hemisphere by applying ring-diagram analysis to the same period of time. They refer to the reverse flow as the “countercell.” Following that discovery, McDonald & Dikpati (2004) presented a meridional circulation model that included multicell formation, which

would prevent the buildup of strong poloidal field predicted by the single-cell meridional circulation dynamo theories.

Describing the meridional circulation profile in depth, as well as its variation with the solar cycle, is one of the major goals of helioseismology (e.g., Basu & Antia 2002; Bogart & Basu 2004). The estimated amplitude of the meridional flows at the base of the convection zone is  $\sim 1.2 \text{ m s}^{-1}$  (Hathaway et al. 2003), too small to be detected by current helioseismic methods. Yet recovering a profile of the circulation to the maximum depth allowed by the observational techniques is crucial for the understanding of the dynamo complexity. Giles (2000) used time-distance helioseismology to search for meridional circulation in the convection zone, and found a poleward flow that extended down to the base of the convection zone. However, by imposing mass conservation on the inversion process of the same observations, he inferred a return point of  $0.8 R_{\odot}$  and an equatorward flow of  $3 \text{ m s}^{-1}$  at the base of the convection zone.

Local helioseismology techniques are limited in the depth range that they can probe. In particular, ring-diagram analysis uses a plane-wave approximation to obtain the temporal and spatial frequencies of modes that propagate in the studied area (Hill 1988), but this approximation is only valid for high- $l$  modes that do not penetrate beyond a certain depth in the solar interior. Extending the analyzed area allows us to include a set of modes in the medium- $l$  range. However, there is a trade-off between the size of the area and the validity of the plane-wave approximation used by the technique, since independently of the  $l$  range, the waves behave as plane waves only in localized small areas over the solar surface.

Figure 1 shows a comparison between the set of modes in the range  $l = 0\text{--}600$  fitted using a  $15^{\circ}$  and a  $30^{\circ}$  (large-aperture)

<sup>1</sup> Operated by the Association of Universities for Research in Astronomy, Inc. under cooperative agreement with the National Science Foundation.

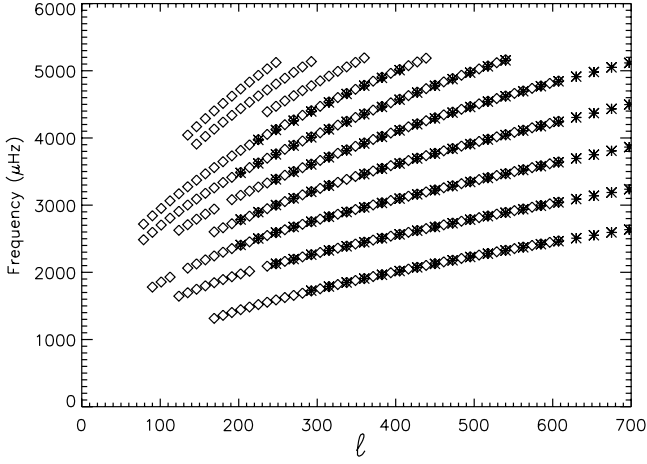


FIG. 1.—Comparison between the set of modes in the  $l$  range of 0–600 fitted using a  $15^\circ$  diameter area (stars) and the ones fitted when using a  $30^\circ$  diameter area (squares).

area tracked over a period of 1664 minutes. Notice that modes in the  $l$  range of 100–200 are only recovered with the larger area. We are particularly interested in these modes for this study, since they penetrate deeper into the solar interior. For the typical  $15^\circ$  diameter area, which can provide information for modes with spherical harmonic degree greater than 175, the resulting inferred velocity flows extend down to about  $0.977 R_\odot$ , about 16 Mm below the solar surface. With the extra modes recovered when using the larger areas, we can survey the solar interior down to about 26 Mm or  $0.96 R_\odot$ . We consider this extra 10 Mm of information valuable and have used the large-aperture ring diagrams approach for our study. Most of the work has been done using a customized version of the Global Oscillation Network Group (GONG) Ring Diagram Pipeline (Corbard et al. 2003).

## 2. DATA ANALYSIS

The data used for this work were obtained by the GONG network. Since the project upgraded the CCD cameras in early 2001 to a  $1024 \times 1024$  pixel array (Harvey et al. 1996), the data can now be used in a local helioseismology context. In addition, the continuous flow of the data makes them appropriate for long term variability studies. The images are full-disk Dopplergrams in the Ni I line (6768 Å), with a cadence of 1 minute and a spatial resolution of  $\sim 5''$  (pixel size of  $\sim 2''.5$ ). We also compare part of

the results with those obtained using the Michelson Doppler Imager (MDI) on the *Solar and Heliospheric Observatory* (SOHO) satellite for the period of time spanning Carrington rotations 1987, 1988, and 1989. The MDI Dopplergrams used have a resolution similar to GONG.

The method used for the study is a variation of the standard ring-diagram analysis, where the studied regions are bigger in area than the standard ones. The ring-diagram method studies high- $l$  degree waves propagating in localized areas over the solar surface to obtain an averaged horizontal velocity vector for that particular region. Analyzing a mosaic of these areas produces a three-dimensional velocity map in the depth range where the modes resonate radially. We have applied ring-diagram analyses to  $32 \text{ deg}^2$  solar areas as they crossed the central meridian. These areas are about 4 times the size of the typically studied areas of  $15 \text{ deg}^2$  (González Hernández et al. 1999).

We track each region with a surface rotation rate at its center given by the equation

$$\Omega(\phi) = \sum_{h=0,2,4} a_h \cosh(\phi) + S_0, \quad (1)$$

where  $\phi$  is the colatitude,  $a_h$  is the coefficient given by (Snodgrass 1984), and  $S_0$  is the sidereal-to-synodic correction. Since we assume the acoustic waves to be plane waves traveling across the surface of the Sun following great circles, we use a transverse cylindrical projection to project the area so that the horizontal and vertical lines approximate great circles. Although the equidistance in this case can only be assured in one direction, the distortion is not too big in the other direction. The tracked and remapped areas are then stored in three-dimensional files called “dense-packs.”

The regions are apodized using a cosine-bell function into  $30^\circ$  diameter areas, and a three-dimensional fast Fourier transform (FFT) is applied to each dense-pack in both spatial and temporal directions to obtain a three-dimensional power spectrum. Cuts at a specific temporal frequency of this large-aperture ring diagram can be seen in Figure 2. We fit the corresponding power spectrum using a Lorentzian profile model described by Haber et al. (2002). The model includes a perturbation term due to the horizontal velocity flows in the region where the fitted mode propagates:  $(k_x V_x + k_y V_y)$ , where  $k_x$  and  $k_y$  are the components of the horizontal wavenumber in the zonal ( $x$ ) and meridional ( $y$ ) directions. Finally, we invert the velocities obtained from the fitting process [ $U_x(l, \nu)$ ,  $U_y(l, \nu)$ ] using a least-squares

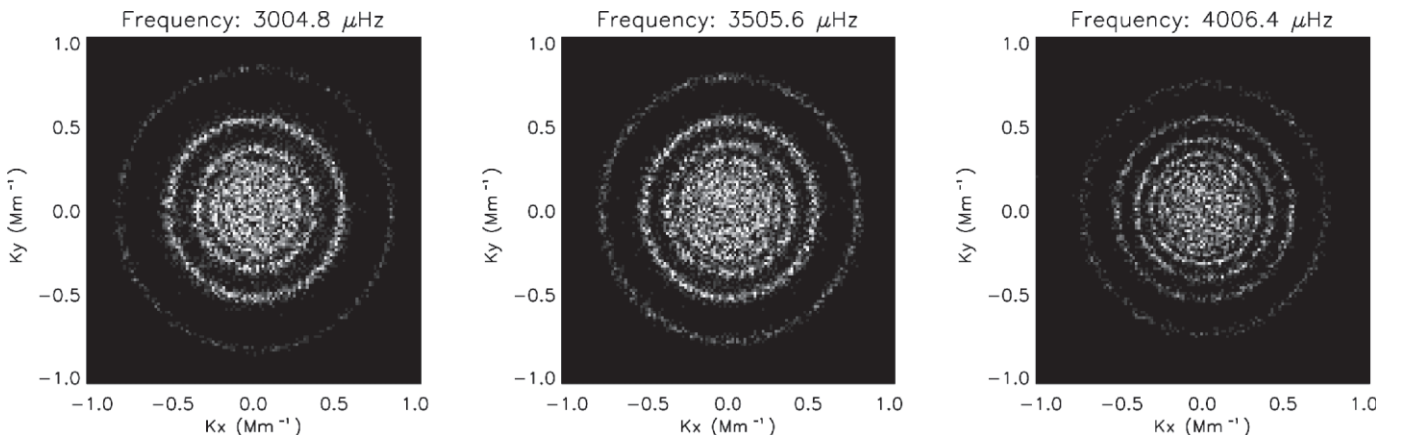


FIG. 2.—Cuts at different frequencies of the three-dimensional power spectrum from one of the  $30^\circ$  diameter areas.

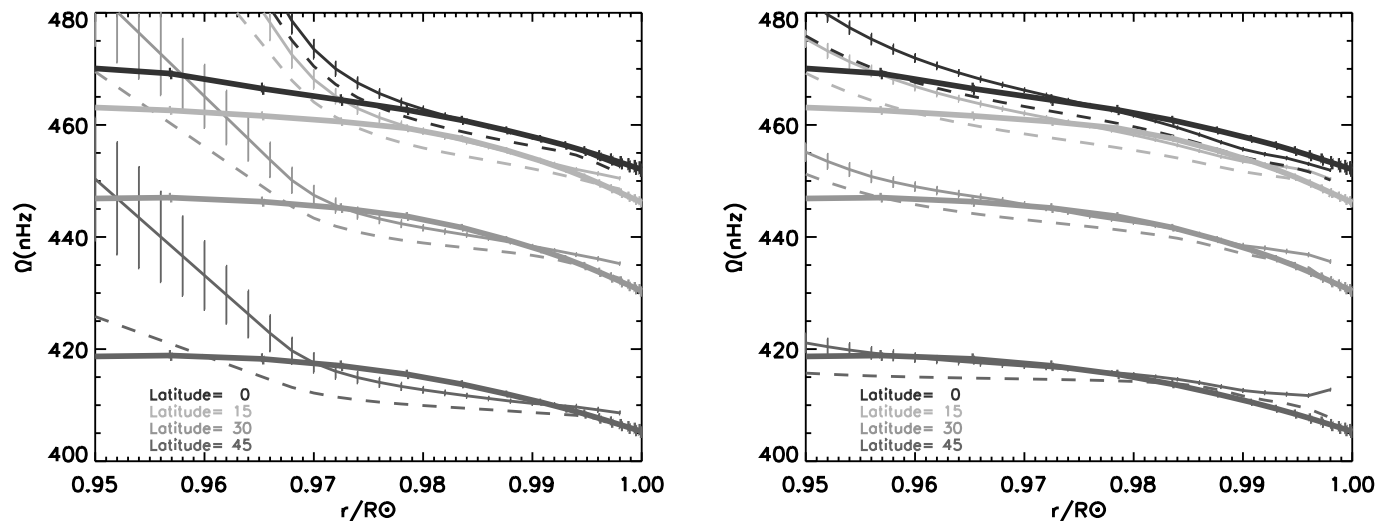


FIG. 3.—Rotation rate for several latitudes ( $0^\circ$ ,  $15^\circ$ ,  $30^\circ$ , and  $45^\circ$ ) from global analysis (*thick solid line*) and from ring diagrams (GONG, *thin solid line*; MDI, *thin dashed line*). The left panel shows the results obtained using the typical  $15^\circ$  diameter areas, the right panel the same results using the larger  $30^\circ$  diameter areas.

inversion method to recover the depth dependence of the horizontal velocity flows [ $v_x(r)$ ,  $v_y(r)$ ].

Through the 2 yr period of data, we look at a set of 15 overlapping sections centered at latitudes  $0^\circ$ ,  $\pm 7.5^\circ$ ,  $\pm 15^\circ$ ,  $\pm 22.5^\circ$ ,  $\pm 30^\circ$ ,  $\pm 37.5^\circ$ ,  $\pm 45^\circ$ , and  $\pm 52.5^\circ$ . We used the regions only as they crossed the central meridian, to minimize the projection effects. The areas are tracked for intervals of 1664 minutes, and the areas located at the same latitude are averaged for every Carrington rotation.

In order to validate the horizontal flows obtained with our large-aperture areas, we compare the differential rotation obtained by averaging the zonal component of the horizontal velocity vectors for Carrington rotation 1989 with the global one obtained for a 3 month series surrounding that Carrington rotation. Figure 3 shows the comparison between the rotation rate obtained using the ring analysis with both  $15^\circ$  and  $30^\circ$  areas using both GONG and MDI data and the rotation rate from the global analysis. It can be seen that the larger-aperture rings provide a more accurate measurement of the rotation rate for deeper layers. There is a clear improvement in the results when the larger areas are used. The continuous increase of the rotation below a certain depth is probably due to the inversion technique; however, the systematic displacement between GONG and MDI results is still under investigation and is discussed in the following section.

### 3. MERIDIONAL CIRCULATION VARIABILITY

We use the  $v_y$  component of the averaged horizontal velocity flows from the set of areas described in the previous section to study the meridional circulation. Figure 4 presents the meridional flows obtained at six different depths for the 25 Carrington rotations (1985–2009). The flows are represented as contours, where dashed lines correspond to negative values (a material motion toward the northern hemisphere is taken as positive). The chosen depths are interpolated from the actual grid given by the inversion.

It can be seen that the amplitude of the flows increases toward the interior of the Sun in the depth range studied. The maximum amplitude very near the surface ( $0.99 R_\odot$ ) is close to  $15 \text{ m s}^{-1}$  and increases gradually to  $30 \text{ m s}^{-1}$  at a depth of about 26 Mm ( $0.96 R_\odot$ ). This is in contrast to the meridional circulation profile used for dynamo modeling, in which meridional circulation

is usually assumed to decrease monotonically from the solar surface down to the base of the convection zone where the equatorward return of the flow is expected to happen (Dikpati & Charbonneau 1999). In a recent paper, Chou & Lodenkov (2005) also find an increase of the meridional circulation with depth for layers below  $0.96 R_\odot$  for a similar period of time by using the time-distance technique. Since the density increases from the surface toward the interior of the Sun, the meridional flow amplitude cannot continue to increase with depth. A shear layer close to the surface, such as the one found in the zonal rotation, might explain our observations.

The maximum amplitude of the meridional flow peaks at about  $25^\circ$  latitude in both hemispheres, but it varies with time (see Fig. 5). We also find that the latitude of the maximum varies with depth. Figure 6 presents the latitude of the maximum meridional flow for each rotation at three depths. Both the individual results for northern (*squares*) and southern (*stars*) hemispheres, as well as the average (*solid line*), are presented. We find no clear variation of the location with time at our maximum explored depth,  $0.96 R_\odot$ ; however, this location seems to be moving slightly toward higher latitudes in the 2 yr period in layers close to the surface ( $0.99 R_\odot$ ). This temporal variation of the latitude of the maximum was also found by Giles (2000).

From about  $0.975 R_\odot$  down, a second cell of meridional circulation appears for four periods centered in Carrington rotations 1987, 1992, 2001, and 2007. Haber et al. (2002) reported a second cell from the north pole toward the equator above  $30^\circ$  when analyzing MDI data with a standard ring-diagram method. In their results, the countercell extended from 5 Mm ( $0.99 R_\odot$ ) down. We also find this northern hemisphere countercell, but at deeper depths. However, countercells in the northern and southern hemisphere can be seen coinciding with maximum values of the solar  $B_0$  angle, the angle of the solar rotation axis toward Earth (see Fig. 7).

Using the continuity equation, we can derive the vertical component of the flows from the calculated divergence of the measured horizontal flows (Komm et al. 2004). Figure 8 presents the velocities resulting from combining the meridional component of the averaged horizontal velocity flows with the calculated vertical component for three Carrington rotations where countercells appear in the northern (CR 1987) and southern (CR 2007) hemispheres, and where there is no obvious countercell (CR 2004).

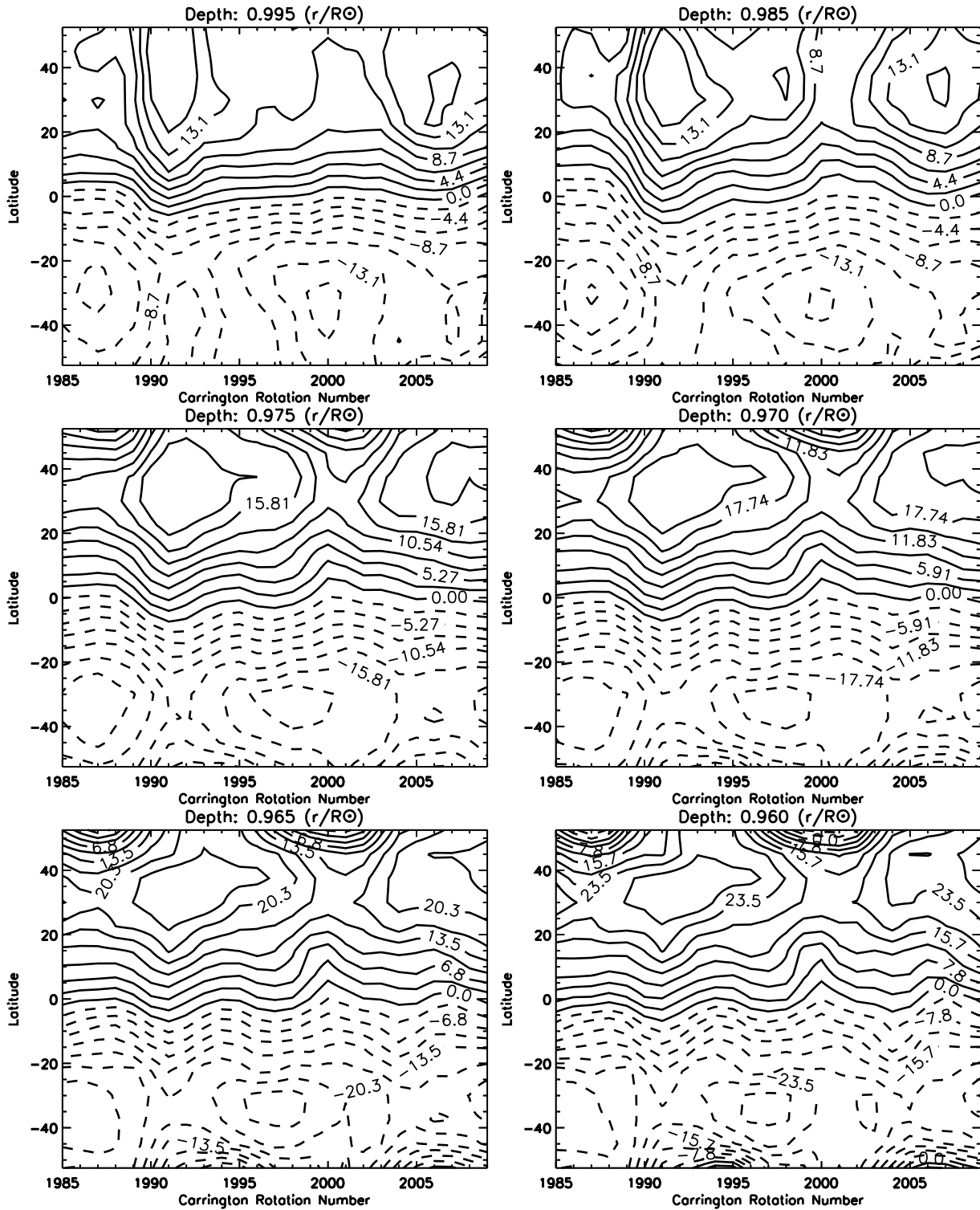


FIG. 4.—Evolution of meridional circulation at six depths during a 2 yr period, 2002 January–2003 December, derived from large-aperture ring-diagram analysis of the GONG continuous data. The contour range varies for each depth; the maximum amplitude increases with depth. Solid lines correspond to positive values (flows toward the north pole) and dashed lines to negative values. Counter cells in the northern and southern hemisphere can be seen appearing with a periodicity of 1 yr.

Beck & Giles (2005) have very recently proposed that an error in the Carrington elements used to calculate the  $P$  and  $B_0$  angles could cause a 1 yr periodic variation of the meridional flows obtained from time-distance helioseismology. They also conclude that a systematic  $P$  angle alignment error, such as the one found in the MDI instrument ( $\sim 0^\circ.17$ ), results in a systematic meridional component superposed on the solar cir-

ulation, due to leakage of zonal rotation into the meridional component.

We have used the large-aperture ring diagrams to calculate the meridional flows for Carrington rotations 1987–1989 from MDI data. The comparison between the GONG and MDI results is shown in Figure 9. It shows a systematic displacement between GONG and MDI results in the meridional flows of approximately

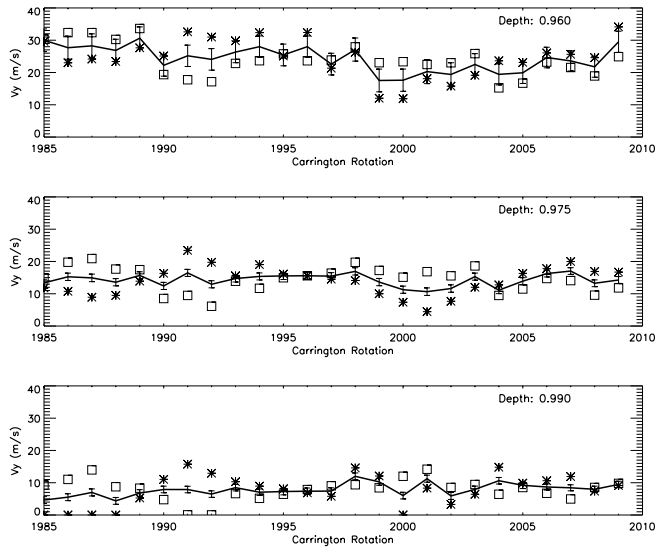


FIG. 5.—Time variation of the maximum amplitude of the meridional flows at three depths. The figures show the average of the north and south hemisphere (solid line) and the independent hemisphere results (squares, north; stars, south).

$-5 \text{ m s}^{-1}$  for most depths and latitudes. An error in the  $P$  angle of  $\Delta P = 0^\circ.17$  accounts for a meridional component at the equator of about  $6 \text{ m s}^{-1}$  [ $\Omega_{\text{equator}} \sin(\Delta P)$ ], explaining the difference between the results from both instruments. However, we also get a discrepancy in the zonal component obtained using data from the GONG and MDI instruments (see Fig. 3). The rotation rate obtained from MDI is consistently lower than that from GONG by approximately  $2 \text{ nHz}$  at all latitudes from the surface down to almost  $0.96 R_\odot$ , although it increases slightly with depth. This difference cannot be explained by the  $P$  angle misalignment in MDI, since the effect in the zonal component at the equator, for example, would be given by  $\Omega_{\text{equator}} [1 - \cos(\Delta P)]$  which is of the order of  $2 \times 10^{-3} \text{ nHz}$ . We also find significant differences below  $0.975 R_\odot$  at high latitudes, where the countercell appears.

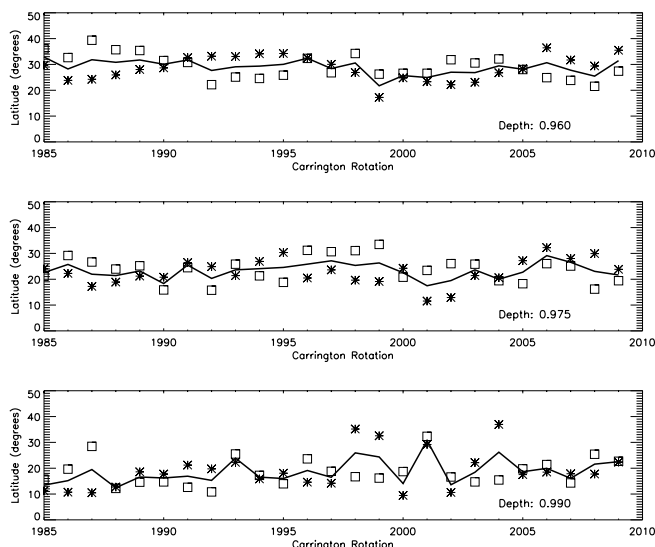


FIG. 6.—Time variation of the latitude of the maximum amplitude of the meridional flows at three depths. The figures show the average of the north and south hemisphere (solid line) and the independent hemisphere results (squares, north; stars, south).

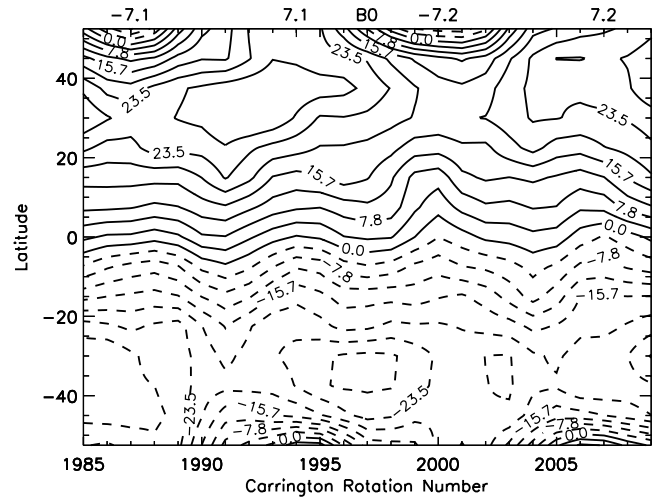


FIG. 7.—Meridional flow contours at  $0.96 R_\odot$  ( $\sim 26 \text{ Mm}$ ). The approximate value of the  $B_0$  angle at the center of Carrington rotations 1987, 1994, 2000, and 2007 has been plotted on the upper axis for reference. Note that the countercells are centered at high values of  $B_0$  (the maximum value of  $B_0$  is  $\sim 7.3$ ), and that this angle varies with a 1 yr periodicity.

The temporal variation of the amplitude of the meridional flows at the equator at three depths from GONG data is shown in Figure 10. Although the amplitude changes significantly through the period of time analyzed, there is no clear offset of the flows from zero, suggesting the absence of significant systematic errors in the GONG  $P$  angle. In addition, Figure 10 does not show the annual variation that would result from an error in the Carrington elements.

Haber & Hindman (2003) show the meridional flows obtained from MDI data that have been corrected from the  $P$  angle error. Although the amplitude of the flows is shifted such that the value at the equator is closer to zero, the northern hemisphere countercell remains visible for all the time spans after 1998 that were analyzed.

Figure 9 reveals a bigger discrepancy between GONG and MDI meridional flow at higher latitudes than the  $6 \text{ m s}^{-1}$  associated with the misalignment. This indicates that we may have other systematic differences between the two sets of data. In a recent paper, Bogart & Basu (2004) described an experiment of applying ring diagrams to a nontracked data cube. The countercell disappears when the solar surface analyzed is centered on the central meridian.

#### 4. DISCUSSION AND CONCLUSIONS

Large-aperture ring diagrams are effective for estimating meridional circulation and differential rotation in layers of the solar interior deeper than those reached by conventional ring-diagram analysis. We are able to recover material motions down to a depth of  $26 \text{ Mm}$  using these larger areas. Although longer series of data would improve the signal-to-noise ratio of the spectrum, allowing the fitting of more modes, there is a limit to the maximum depth observable by current ring-diagram analysis, which is not much larger than that obtained in this work. Preliminary tests using a  $45^\circ$  diameter area show that only a very few extra modes are fitted when expanding the size of the area even further, and that the errors in the fitting of those extra modes increase considerably. In addition, the plane-wave approximation fails for lower spatial frequency modes.

Using larger areas also introduces bigger uncertainties in the projection. This is particularly true near the limb. We believe

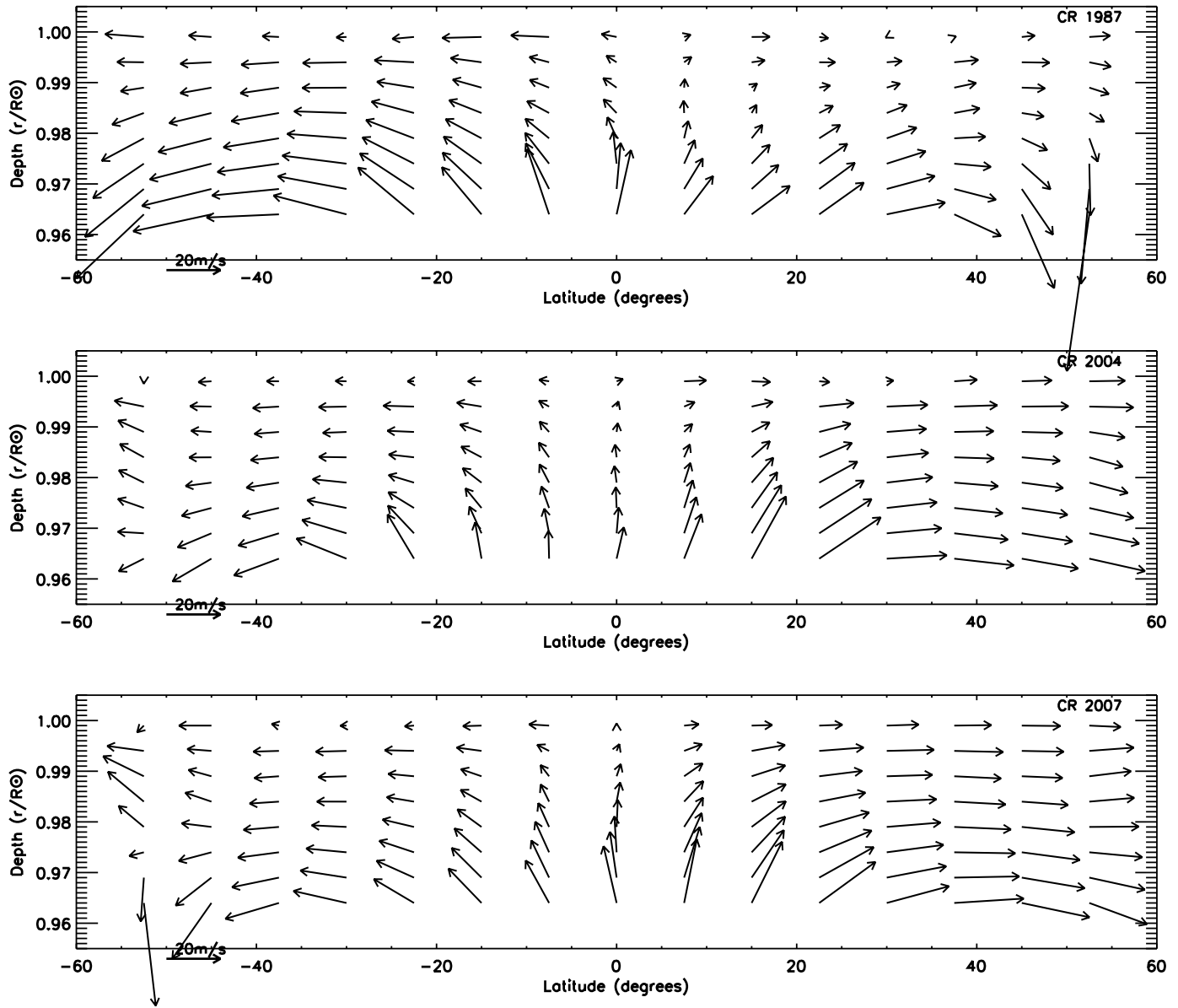


FIG. 8.—Velocity vectors obtained by combining the meridional component of the averaged horizontal velocity flows with the calculated vertical component. The top figure shows the results for CR 1987 with the northern hemisphere counter-cell. The central plot corresponds to CR 2004, where no counter-cell is found, and the bottom to CR 2007, showing a counter-cell in the southern hemisphere.

that these effects systematically affect our results at high latitudes, especially in those periods where the  $B_0$  angle has an extreme value ( $\pm 7.3^\circ$ ).

We do not find a periodic variation of the equator-crossing flows. However, the latitude for the maximum amplitude changes in a range of  $\pm 10^\circ$  in the studied period of time, and the maximum amplitude of the flows varies within  $\pm 5 \text{ m s}^{-1}$ . A variation of the meridional flows with the solar cycle has been reported by Giles (2000) and Chou & Dai (2001) using time-distance analysis, and Basu & Antia (2002) using ring-diagrams. We need to analyze a longer period of time to corroborate their results.

Our results confirm the counter-cell in the northern hemisphere previously reported by Haber et al. (2002), but find a periodic appearance of similar counter-cells in the northern and southern hemisphere that correlates with maximum values of the  $B_0$  angle. We suspect that geometric calibration issues or the analysis method affect the meridional circulation results. This may be due to the larger areas that extend to latitudes where the

foreshortening is high. A thorough investigation is needed to properly determine of how the geometry and projection errors influence ring-diagram analysis in particular, and local helioseismology results in general.

All the results and prospects outlined in the previous section are currently limited in application to the outer 26 Mm of the solar convection zone. Other local helioseismology techniques, such as time-distance analysis, are able to recover information from deeper regions of the Sun, and their results would be very valuable to establish a complete picture of the meridional circulation.

We will continue to apply the technique to GONG data as it is made available to search for a meridional circulation variation with the solar cycle. A previous study by Chou & Dai (2001) using Taiwan Oscillation Network (TON) data found variations that were different for the declining and the rising phase of Cycle 22. They also found a general increase with depth in the meridional flows of up to  $40 \text{ m s}^{-1}$ . Our work agrees with an increase in the magnitude of the meridional flows with depth in the region

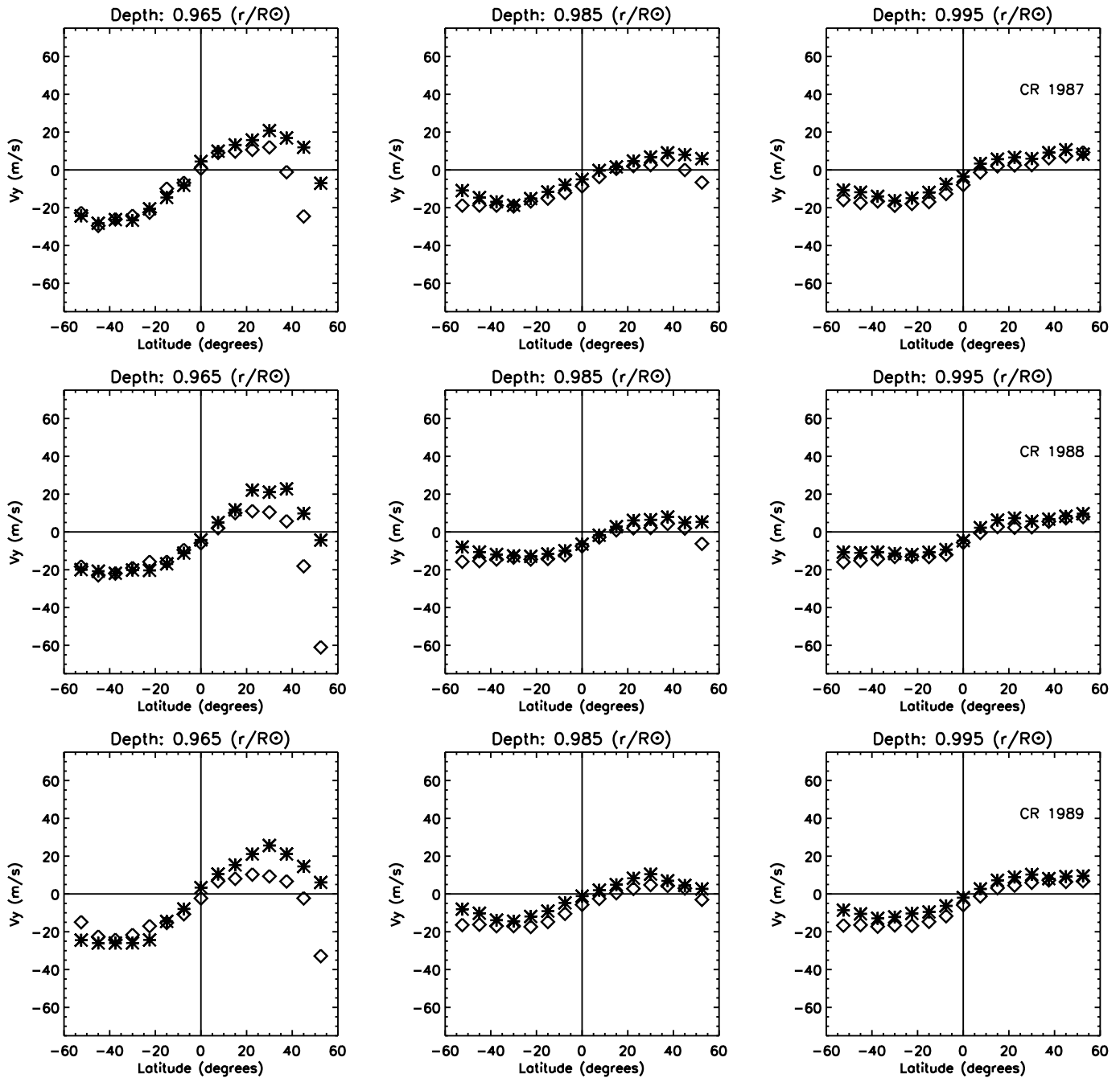


FIG. 9.—Meridional component of the horizontal velocity flows as a function of latitude at three different depths for Carrington rotations 1987 (*top*), 1988 (*middle*), and 1989 (*bottom*). The stars show the results obtained using the GONG instrument data, while the squares represent the results from MDI.

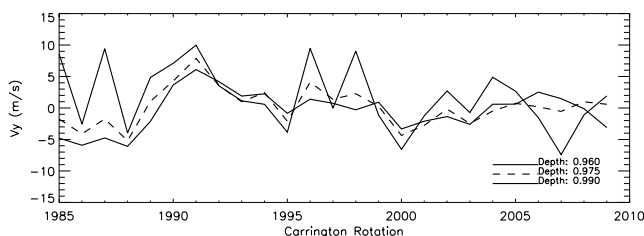


FIG. 10.—Temporal variation of the meridional flow at the equator at three different depths.

analyzed. These results may indicate the presence of a shear layer in the upper layers of the convection zone for the meridional circulation, similar to the one found in the zonal rotation.

The limitations we are encountering when studying areas far from disk center need to be investigated. We expect that with a better understanding of these systematic effects we will be able to calibrate them and shed more light on the existence of a multicell meridional circulation in the Sun.

We thank J. Bolding, R. Bogart, B. Hindman, R. M. Larsen, and C. Toner for their contribution to the ring-diagram pipeline code. This work was supported by NASA grant NAG5-11703.

*SOHO* is a project of international cooperation between ESA and NASA. This work utilizes data obtained by the GONG program, managed by the National Solar Observatory, which is operated by Association of Universities for Research in Astronomy, Inc., under a cooperative agreement with the National Science

Foundation. The data were acquired by instruments operated by the Big Bear Solar Observatory, High Altitude Observatory, Learmonth Solar Observatory, Udaipur Solar Observatory, Instituto de Astrofísica de Canarias, and Cerro Tololo Inter-American Observatory.

## REFERENCES

- Basu, S., & Antia, H. M. 2002, in Proc. SOHO 11 Symposium, ed. A. Wilson (ESA SP-508, Noordwijk: ESA), 151.
- Beck, J. G., & Giles P. 2005, ApJ, 621, L153
- Bogart, R. S., & Basu, S. 2004, in Proc. SOHO 14/GONG 2004 Workshop, ed. D. Danesy (ESA SP-559, Noordwijk: ESA), 329
- Chou, D. Y., & Dai, D. C. 2001, ApJ, 559, L175
- Chou, D. Y., & Ladenkov, O. 2005, ApJ, 630, 1206
- Corbard, T., Toner, C., Hill, F., Haber, D., Bogart, R., & Hindman, B. 2003, in Proc. SOHO 12/GONG+ 2002: Local and Global Helioseismology: The Present and Future, ed. H. Sawaya-Lacoste (ESA SP-517, Noordwijk: ESA), 255
- Dikpati, M., & Charbonneau, P. 1999, ApJ, 518, 508
- Dikpati, M., & Gilman, P. A. 2001, ApJ, 559, 428
- Giles, P. M. 2000, Ph.D. thesis, Stanford Univ.
- Giles, P. M., Duvall, T. L., Jr., Sherrer, P. H., & Bogart, R. S. 1997, Nature, 390, 52
- Gilman, P. A., & Miesch, M. 2004, ApJ, 611, 568
- González Hernández, I., et al. 1999, ApJ, 510, L153
- Haber, D. A., & Hindman, B. W. 2003, Highlights Astron., 13, 44
- Haber, D. A., Hindman, B. W., Toomre, J., Bogart, R. S., Larsen, R. M., & Hill, F. 2002, ApJ, 570, 255
- Harvey, J. W., et al. 1996, Science, 272, 1284
- Hathaway, D. H., Nandy, D., Wilson, R. M., & Reichmann, E. J. 2003, ApJ, 589, 665
- Hathaway, D. H., et al. 1996, Science, 272, 1306
- Hill, F. 1988, ApJ, 333, 996
- Komm, R., Corbard, T., Durney, B. R., González Hernández, I., Hill, F., Howe, R., & Toner, C. 2004, ApJ, 605, 554
- Komm, R. W., Howard, R. F., & Harvey, J. W. 1993, Sol. Phys., 147, 207
- McDonald, E., & Dikpati, M. 2004, BAAS, 36, 756
- Nandy, D., & Choudhuri, A. R. 2002, Science, 296, 1671
- Nesme-Ribes, E., Meunier, N., & Vince, I. 1997, A&A, 321, 323
- Snodgrass, H. B. 1984, Sol. Phys., 94, 13
- Snodgrass, H. B., & Dailey, S. B. 1996, Sol. Phys., 163, 21